J Biomol NMR (2017) 68:249–255
DOI 10.1007/s10858-017-0122-9

ARTICLE

An enhanced sensitivity methyl ^{1}H triple-quantum pulse scheme for measuring diffusion constants of macromolecules

Rui Huang[1] · Jacob P. Brady[1] · Ashok Sekhar[1] · Tairan Yuwen[1] · Lewis E. Kay[1,2]

Received: 25 April 2017 / Accepted: 21 June 2017 / Published online: 17 July 2017

Abstract We present a pulse scheme that exploits methyl ^{1}H triple-quantum (TQ) coherences for the measurement of diffusion rates of slowly diffusing molecules in solution. It is based on the well-known stimulated echo experiment, with encoding and decoding of TQ coherences. The size of quantifiable diffusion coefficients is thus lowered by an order of magnitude with respect to single-quantum (SQ) approaches. Notably, the sensitivity of the scheme is high, approximately ¾ that of the corresponding single quantum experiment, neglecting relaxation losses, and on the order of a factor of 4 more sensitive than a previously published sequence for AX_3 spin systems (Zheng et al. in JMR 198:271–274, 2009) for molecules that are only ^{13}C labeled at the methyl carbon position. Diffusion coefficients measured from TQ- and SQ-based experiments recorded on a range of protein samples are in excellent agreement. We present an application of this technique to the study of phase-separated proteins where protein concentrations in the condensed phase can exceed 400 mg/mL, diffusion coefficients can be as low as ~10^{-9} cm^2s^{-1} and traditional SQ experiments fail.

Keywords Diffusion · NMR · Triple-quantum · Methyl groups · Ddx4

Electronic supplementary material The online version of this article (doi:10.1007/s10858-017-0122-9) contains supplementary material, which is available to authorized users.

✉ Lewis E. Kay
kay@pound.med.utoronto.ca

[1] Departments of Molecular Genetics, Biochemistry and Chemistry, University of Toronto, Toronto, ON M5S 1A8, Canada

[2] The Hospital for Sick Children Research Institute, Toronto, ON M5G 0A4, Canada

Introduction

Pulse field gradient (PFG) NMR spectroscopy (Stejskal and Tanner 1965; Johnson 1999) is a well-established tool for the measurement of translational diffusion coefficients of protein molecules in solution (Yao et al. 2014). The obtained diffusion constants can, in turn, be used to gain insight into a variety of important biochemical processes, including, for example, protein oligomerization (Dingley et al. 1995; Price et al. 1999; Dehner and Kessler 2005; Huang et al. 2016), conformational changes (Buevich and Baum 2002; Choy et al. 2002; Weljie et al. 2003), ligand binding (Hajduk et al. 1997; Yan et al. 2002) and the formation of molecular complexes (Didenko et al. 2011; Horst et al. 2011; Sekhar et al. 2015). The measurement of diffusion coefficients in PFG-based NMR experiments is based on the application of a PFG that labels the initial position of diffusing molecules, followed by a second gradient that is applied after a period during which the molecules diffuse that encodes the extent of diffusion through an attenuation of signal intensity (Tanner 1970). Key to the success of the experiment is the use of well-tuned diffusion times and PFG strengths and durations that lead to the diffusion-based attenuation of the signals of interest so that diffusion coefficients can be reliably quantified. In applications to slowly diffusing systems using conventional hardware this presents a significant challenge since gradient strengths and often durations are limited.

One approach to mitigate the problem is to take advantage of stimulated echo (STE) based experiments (Tanner 1970), with the diffusion interval occurring when the magnetization of interest is along the *z*-axis, so as to exploit the large difference in longitudinal and transverse relaxation rates for macromolecules. Another approach involves the design of long-lived coherences that has proven to be a powerful method for extending diffusion intervals, leading

to increased gradient attenuation (Ahuja et al. 2009). In a somewhat related manner it is possible to take advantage of moieties in proteins such as methyl groups, that have favorable relaxation properties, and further that can be manipulated in ways that increase the effective sensitivity of PFGs for the measurement of diffusion. For example, it is well known that the effect of gradients on coherences of order n scales as n^2 (Martin et al. 1982; Zax and Pines 1983; Kay and Prestegard 1986), and the three protons of the methyl AX_3 spin system offer, therefore, an attractive opportunity to generate a triple-quantum (TQ) based diffusion experiment, with close to an order of magnitude enhancement in attenuation from diffusion. Indeed, Price and coworkers have developed a four-quantum scheme based on $^{13}CH_3$ labeled methyl groups and showed the desired response to the application of PFGs (Zheng et al. 2009). Our work follows closely on their approach but offers at least a factor of 4 increase in sensitivity that is critical for biomolecular applications (see below).

Our interest in the development of a sensitive pulse scheme for the measurement of slow diffusion rates is motivated by our studies of the hydrodynamic properties of intrinsically disordered proteins that phase separate into membraneless cellular organelles (Brangwynne et al. 2015). In some cases these phase-separated molecules retain high levels of intrinsic dynamics on the pico- to nano-second timescale, yet diffuse with rates that are expected for a 600 nm spherical particle (Nott et al. 2015; Brady et al. 2017). An understanding of the properties that give rise to such slow diffusion would represent an important step forward in characterizing the physical basis for the formation of these organelles and how they are stabilized. With this in mind we present a pulse scheme for the measurement of translational diffusion coefficients of slowly diffusing proteins that takes advantage of TQ coherences from methyl groups. The utility of the approach is demonstrated with applications to a number of systems where both SQ and TQ diffusion experiments are operative. Subsequently, we have applied our pulse scheme to the measurement of diffusion rates in a 236-residue fragment of the germ granule protein Ddx4 that spontaneously phase separates to form a highly concentrated, condensed phase (300–400 mg/mL) and for which reliable diffusion coefficients cannot be extracted by conventional SQ PFG-NMR methods.

Materials and methods

Protein expression and purification

A highly deuterated Ileδ1-[$^{13}CH_3$], Leu,Val-[$^{13}CH_3$,$^{12}CD_3$]-labeled B1 domain of peptostreptococcal protein L with a Y45W mutation (referred to as protein L in what follows) and a U-[^{13}C,^{15}N]-labeled protein L sample were prepared as described previously (Mittermaier and Kay 2001; Bouvignies and Kay 2012). Protein concentrations were 1.2 and 1.8 mM for the ILV-methyl-labeled and uniformly ^{13}C,^{15}N-labeled protein L samples, respectively, dissolved in 50 mM sodium phosphate, 0.05% NaN_3, 99% D_2O (ILV-methyl-labeled) or 90% H_2O/10% D_2O (U-[^{13}C,^{15}N]-labeled), pH 6.0. A U-^{2}H, Ileδ1-[$^{13}CH_3$], Leu,Val-[$^{13}CH_3$,$^{12}CD_3$], Met-[$^{13}CH_3$]-labeled sample of the half proteasome ($\alpha_7\alpha_7$, 360 kDa) was prepared as described previously (Sprangers and Kay 2007). The protein concentration of the half proteasome sample was 0.9 mM, in 25 mM potassium phosphate, 50 mM NaCl, 4.6 mM NaN_3, 1 mM EDTA, 100% D_2O, pH 7.4.

Samples of wild-type human Ddx4(1-236) (referred to in what follows as Ddx4) and Ddx4 in which all 14 Phe residues were replaced by Ala, $Ddx4_{14FtoA}$, were prepared as described previously (Nott et al. 2015). *E. coli* codon optimized cysteine free (Cys to Ser) Ddx4 concatemers ($Ddx4_{2x}$ and $Ddx4_{3x}$, containing 2 and 3 Ddx4 repeats, respectively) were synthesized (Genscript) and sub-cloned into pET-SUMO vectors. Briefly, N-terminal His-SUMO constructs were expressed in *E. coli* and cell pellets were lysed in the presence of 6 M guanidinium HCl (GuHCl), 500 mM NaCl, 50 mM sodium phosphate, pH 7.5. Samples were purified using pre-packed nickel Sepharose columns and eluted with 400 mM imidazole, 1 M NaCl, 50 mM sodium phosphate, pH 7.5. His-SUMO tags were cleaved using Ulp1 during an overnight dialysis in 10 mM imidazole, 1 M NaCl, 50 mM sodium phosphate, pH 7.5, 4 °C. Ddx4 constructs were then separated from His-SUMO fragments and Ulp1 by reapplication to a nickel-Sepharose column and the resulting samples concentrated in 2 M GuHCl, 1 M NaCl, 50 mM sodium phosphate, pH 7.5 using 3 kDa molecular weight cut off (MWCO) concentrators before size-exclusion chromatography in 1 M NaCl, 50 mM sodium phosphate, pH 6.5. For $Ddx4_{3x}$, size-exclusion chromatography was performed in the presence of 2 M GuHCl to prevent phase separation from occurring on the column. After purification, unlabeled samples were doped with 10% U-[^{13}C,^{15}N]-labeled protein to facilitate NMR analysis. NMR samples of phase separated Ddx4, $Ddx4_{2x}$ and $Ddx4_{3x}$ were prepared by dialysis into buffer containing 20 mM sodium phosphate, 100 mM NaCl, 5 mM TCEP, 10% D_2O, pH 6.5. For $Ddx4_{14FtoA}$, samples were exchanged into buffer containing 20 mM sodium phosphate, 100 mM NaCl, 5 mM TCEP, 90%H_2O/10%D_2O, pH 6.5 and concentrated using 4-mL 3-kDa cut-off MWCO Amicon Ultra filters at 4000 g, 25 °C. All samples were subsequently transferred into 3 mm NMR tubes (Wilmad), gently centrifuged, and allowed to equilibrate at 30 °C for a minimum of 24 h to ensure that the condensed droplets coalesce to a homogeneous phase. Care was taken to ensure that the condensed

phase filled the NMR coil volume (and beyond). It is worth noting in this regard that phase separated samples of Ddx4 can be visually identified as having two phases, so that it is not difficult to ensure that only the condensed phase is in the active region of the coil. The great majority of the dilute phase (that is above the condensed phase) is typically removed from the sample prior to experiments.

NMR data acquisition and processing

All NMR experiments were performed on a Bruker Avance III HD 14.0 T spectrometer, equipped with a cryogenically cooled *x,y,z*-pulsed field gradient triple resonance probe. 1D experiments were recorded at 25 °C for protein L and $\alpha_7\alpha_7$, and at 30 and 35 °C for Ddx4, $Ddx4_{2x}$, $Ddx4_{3x}$ and $Ddx4_{14FtoA}$ samples, using either a SQ-based pulse scheme with ^{15}N and ^{13}C pulses interchanged (Choy et al. 2002) or the TQ-based sequence of Fig. 1. Diffusion constants were obtained by integrating ^1H signals in 1D experiments, recorded as a function of encoding/decoding gradient strengths, over frequency ranges extending from −0.2 to 1.3 ppm, from 1.90 to 2.10 ppm and from 1.95 to 2.07 ppm for protein L, $\alpha_7\alpha_7$ and Ddx4, respectively. Diffusion constants were obtained by non-linear least-squares fits of intensity data via Eq. 3 using calibrated gradient intensity values that were obtained from diffusion experiments of HOD in a D_2O solution at 25 °C where the diffusion of HOD is known (Price 1998).

Results and discussion

Figure 1 illustrates the TQ-based pulse scheme that we have developed for measurement of diffusion constants in biomolecules. In order to highlight the important elements of the sequence we first briefly outline the magnetization transfer pathway as follows,

$$
\begin{aligned}
&\mathrm{H}_z^1 \xrightarrow{90^\circ_x(\mathrm{H})} \mathrm{H}_y^1 \xrightarrow{\tau_a 180^\circ(\mathrm{H})180^\circ(\mathrm{C})\tau_a} 2\mathrm{H}_x^1\mathrm{C}_z \xrightarrow{90^\circ_x(\mathrm{C})} 2\mathrm{H}_x^1\mathrm{C}_y \\
&\xrightarrow{\tau_b 180^\circ(\mathrm{H})180^\circ(\mathrm{C})\tau_b} 8\mathrm{H}_x^1\mathrm{H}_z^2\mathrm{H}_z^3\mathrm{C}_y \xrightarrow{90^\circ_x(\mathrm{H})90^\circ_x(\mathrm{C})} 8\mathrm{H}_x^1\mathrm{H}_y^2\mathrm{H}_y^3\mathrm{C}_z \\
&\xrightarrow{g_5 180^\circ(\mathrm{H})g_5} -\frac{3}{4}\cos 3\theta \cdot \mathbf{8H_xH_yH_yC_z} + \frac{1}{4}\cos 3\theta \cdot \mathbf{8H_x^1H_x^2H_x^3C_z} \\
&\xrightarrow{90^\circ_x(\mathrm{H})90^\circ_x(\mathrm{C})} \xrightarrow{\tau_b 180^\circ(\mathrm{H})180^\circ(\mathrm{C})\tau_b} \xrightarrow{90^\circ_y(\mathrm{H})90^\circ_x(\mathrm{C})} -\frac{3}{4}\cos 3\theta \cdot 2\mathrm{H}_z^T\mathrm{C}_z + \frac{1}{4}\cos 3\theta \cdot 8\mathrm{H}_z^1\mathrm{H}_z^2\mathrm{H}_z^3\mathrm{C}_z \xrightarrow{\Delta} \\
&\xrightarrow{90^\circ_y(\mathrm{H})90^\circ_x(\mathrm{C})} \xrightarrow{\tau_b 180^\circ(\mathrm{H})180^\circ(\mathrm{C})\tau_b} \xrightarrow{90^\circ_x(\mathrm{H})90^\circ_x(\mathrm{C})} -\frac{3}{4}\cos 3\theta \cdot 8\mathrm{H}_x\mathrm{H}_y\mathrm{H}_y\mathrm{C}_z + \frac{1}{4}\cos 3\theta \cdot 8\mathrm{H}_x^1\mathrm{H}_x^2\mathrm{H}_x^3\mathrm{C}_z \\
&\xrightarrow{g_5 180^\circ(\mathrm{H})g_5} \frac{3}{4}\cos 3\theta \cdot \cos 3\theta' \cdot 8\mathrm{H}_x\mathrm{H}_y\mathrm{H}_y\mathrm{C}_z \xrightarrow{90^\circ_x(\mathrm{H})90^\circ_x(\mathrm{C})} \xrightarrow{\tau_b 180^\circ(\mathrm{H})180^\circ(\mathrm{C})\tau_b} \\
&\xrightarrow{90^\circ_x(\mathrm{C})} \xrightarrow{\tau_a 180^\circ(\mathrm{H})180^\circ(\mathrm{C})\tau_a} \frac{3}{4}\cos 3\theta \cdot \cos 3\theta' \mathrm{H}_y^T
\end{aligned}
\tag{1}
$$

where

$$
\begin{aligned}
8\mathrm{H}_x\mathrm{H}_y\mathrm{H}_y\mathrm{C}_z &= \frac{1}{3}\left\{8\mathrm{H}_x^1\mathrm{H}_y^2\mathrm{H}_y^3\mathrm{C}_z + 8\mathrm{H}_y^1\mathrm{H}_x^2\mathrm{H}_y^3\mathrm{C}_z + 8\mathrm{H}_y^1\mathrm{H}_y^2\mathrm{H}_x^3\mathrm{C}_z\right\} \\
\mathrm{H}_p^T &= \frac{1}{3}\left\{\mathrm{H}_p^1 + \mathrm{H}_p^2 + \mathrm{H}_p^3\right\}
\end{aligned}
\tag{2}
$$

In Eqs. 1 and 2, H_p^q (C_p) $p \in \{x, y, z\}$ denotes ^1H (^{13}C) *p*-magnetization with the superscript $q \in \{1, 2, 3\}$ distinguishing the three identical ^1H spins, the effects of relaxation and pulse imperfections have been neglected, only those terms that are germane to what follows in the pulse scheme are retained (i.e., that ultimately contribute to observable magnetization), the minus signs preceding some of the terms are omitted, $\theta = \gamma g_5 z_1 \delta$, $\theta' = \gamma g_5 z_2 \delta$, γ is the gyromagnetic ratio of a ^1H spin, and z_1 and z_2 are the *z*-positions of the ^1H spins in question at the time of application of encoding (z_1) and decoding (z_2) gradient pairs (g_5), respectively. In Eq. 1 we have included only the case where magnetization begins on proton 1, but an equivalent pair of additional pathways would hold for protons 2 and 3 as well. Further, only the first line of the phase cycle has been assumed, although we explicitly evaluate the effect of the g_5 gradients on the TQ coherences that are a subset of the triple spin ^1H coherences present during the gradient encode/decode periods.

Notably, and quite remarkably, the first TQ selection step does not result in a sensitivity loss in the absence of relaxation. This is because while only ¾ of the starting multi-spin coherence $8\mathrm{H}_x^1\mathrm{H}_y^2\mathrm{H}_y^3\mathrm{C}_z$ is preserved by the TQ filter, an additional term, $8\mathrm{H}_x^1\mathrm{H}_x^2\mathrm{H}_x^3\mathrm{C}_z$ is retained by the selection process that contributes the missing ¼ (*bold* terms in Eq. (1)); note that the terms add constructively, despite their opposite signs, that can be seen by continuing to evolve them during the pulse scheme). During the subsequent Δ delay the diffusing magnetization is longitudinal, either 2 spin- ($2\mathrm{H}_z\mathrm{C}_z$) or 4 spin- ($8\mathrm{H}_z\mathrm{H}_z\mathrm{H}_z\mathrm{C}_z$) order. It is possible

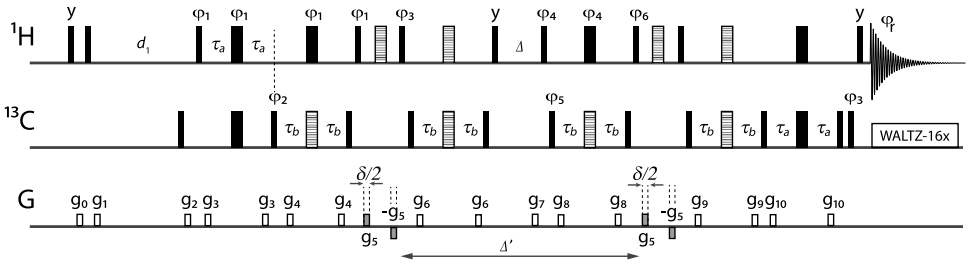

Fig. 1 Pulse scheme of the ^{13}C-methyl select ^{1}H TQ-based stimulated echo diffusion experiment. All *narrow* and *wide bars* correspond to 90° and 180° pulses, respectively, applied at maximum power with phase x unless otherwise indicated; *hatched rectangles* denote composite 180° pulses (Levitt and Freeman 1979). ^{1}H and ^{13}C transmitters are placed in the center of the methyl region (1.0 ppm for ^{1}H and 20.0 ppm for ^{13}C). The 90_y–g_0–90_x–g_1– element prior to the recovery delay, d_1, dephases any residual magnetization from the previous scan. Water suppression can be achieved via presaturation during d_1 or by a WATERGATE scheme during the final INEPT element (Sklenar et al. 1993). The delays are $\tau_a = \tau_b = 2$ ms with Δ and δ adjusted for each sample. Gradients are applied with the following durations (ms) and strengths (G/cm): g_0: (0.75, 6.75), g_1: (0.75, 13.5), g_2: (0.5, 9), g_3: (0.3, 4.5), g_4: (0.256, 6.75), g_6: (0.4, −2.25), g_7: (0.75, 27), g_8: (0.3, −4.5), g_9: (0.3, −6.75), g_{10}: (0.256, 4.5). Gradient g_5 is used for encoding/decoding; its strength is varied in a set of 1D experiments. The following phase cycling is employed: $\varphi_1 = \{0°, 60°, 120°, 180°, 240°, 300°\}$, $\varphi_2 = \{36(x), 36(-x)\}$, $\varphi_3 = \{18(x), 18(-x)\}$, $\varphi_4 = \{6(90°), 6(150°), 6(210°), 6(270°), 6(330°), 6(30°)\}$, $\varphi_5 = \{18(x), 18(-x)\}$, $\varphi_6 = \{6(0°), 6(60°), 6(120°), 6(180°), 6(240°), 6(300°)\}$, $\varphi_r = \{3(x, -x), 3(-x, x), 6(x, -x), 3(-x, x), 3(x, -x), 3(-x, x), 3(x, -x), 6(-x, x), 3(x, -x), 3(-x, x)\}$

to refocus magnetization further to H_z and $4H_zH_zH_z$, with H_z expected to have more favorable relaxation properties than the other longitudinal terms, at the expense of an additional INEPT element both before and after Δ. In applications to a number of systems we have found that in some cases refocusing to *z*-magnetization is preferable for Δ values on the order of 150 ms or larger. Both options are available in the pulse code that is included in Supporting Information. Finally, at the end of the gradient decode element [second of the $g_5180°(^1H)g_5$ pair] only terms of the form $8H_xH_yH_yC_z$ ultimately lead to observable magnetization, corresponding to retention of ¾ of the starting magnetization [Eq (1)]. The theoretical ¼ sensitivity loss that is predicted in Eq. (1) has been verified experimentally by comparing signal-to-noise values (s/n) in spectra recorded of 2-^{13}C acetate with the scheme of Fig. 1 and with a nearly identical scheme where the phase cycling has been modified such that all ^{1}H pulse phases are fixed to the first value of the phase cycle that effectively removes the TQ filters. The resulting s/n is indeed reduced to ¾ of the initial value.

The net signal can be calculated by integrating the product $\cos 3\theta \cos 3\theta'$ over the complete sample volume taking into account the probability of finding the diffusing molecule at positions z_1 and z_2 at the start and finish of the diffusion period, respectively. This gives the well-known expression for the attenuation of magnetization from diffusion,

$$I = I_0 \exp(-n^2\gamma^2 g_5^2 \delta^2 D\Delta'); \; \Delta' \gg \delta \qquad (3)$$

where $n = 3$. We have measured relative signal-to-noise values for the pulse scheme of Fig. 1 and a previously developed experiment that encodes and decodes 4-quantum coherences ($H^1_+H^2_+H^3_+C_+$, $H^1_-H^2_-H^3_-C_-$) using a variety of test samples ranging from acetate to $\alpha_7\alpha_7$. Sensitivity gains on the order of a factor of 4 are obtained for the present experiment when molecules are labeled with ^{13}C only in the methyl position and in the limit that $\Delta' \rightarrow 0$ (Figure S1A). Losses in the 4-quantum experiment result principally from selecting 4-quantum over 3-quantum coherences and the use of a gradient coherence selection scheme as opposed to phase cycling (Zheng et al. 2009). Notably, applications to uniformly ^{13}C labeled proteins establish much more significant sensitivity loses with the 4-quantum experiment, in excess of an order of magnitude, that arise from evolution due to the one-bond $^{13}C_{methyl}$–^{13}C couplings during the lengthy delays in the pulse scheme (Figure S1B); Met residues do not suffer this loss. However, the 4-quantum experiment does offer modest improvements in studies of slowly diffusing molecules, with $n = 3.25$ ($=[3\gamma_H + \gamma_C]/\gamma_H$), such that similar levels of signal attenuation are obtained in applications of the 4- and 3-quantum experiments for systems with diffusion constants in the ratio of 0.85:1, respectively.

As a first test of the methodology we measured diffusion constants for protein L, a small protein of 63 residues, using both the standard SQ experiment of Choy et al. (Choy et al. 2002) and the TQ scheme of Fig. 1. A comparison of signal intensities with very small diffusion times and $g_5 = 0$ shows that ~50% of the signal is preserved in the TQ scheme relative to the SQ experiment when applied to protein L, that includes losses due to the TQ selection elements as well as from relaxation during the increased number of delays in the pulse sequence. Experiments were recorded on both ^{2}H, Ileδ1-[$^{13}CH_3$],Leu,Val-[$^{13}CH_3$,$^{12}CD_3$]-labeled (Fig. 2a) and uniformly [^{13}C,^{15}N]-labeled (Fig. 2b) samples, where in the latter case methyl-only spectra were obtained via TQ selection. Figure 2 shows intensity profiles, obtained from

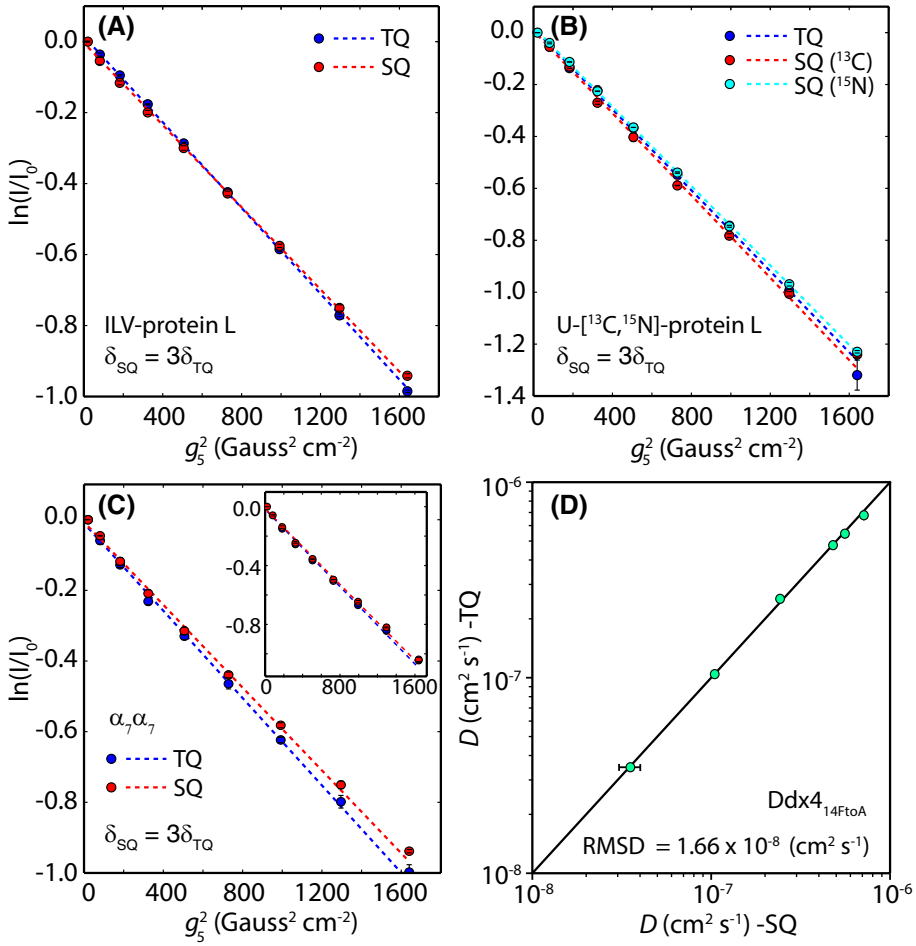

Fig. 2 **a** Intensity profiles as a function of encoding/decoding gradient squared for a sample of ^{2}H, Ileδ1[$^{13}CH_3$], Leu,Val-[$^{13}CH_3$,$^{12}CD_3$]-labeled protein L measured using SQ—(*red*) or TQ—(*blue*) based diffusion experiments, 25 °C. Extracted diffusion constants are $(1.01\pm0.01)\times10^{-6}$ and $(1.06\pm0.01)\times10^{-6}$ cm^{2}s^{-1} from SQ and TQ measurements, respectively, with errors given by the maximum of either the standard deviation based on triple repeat experiments or errors from individual fits. **b** As in **a** but for a U-[^{13}C,^{15}N]-labeled protein L sample with measurements via 1D ^{13}C-edited SQ—(*red*), ^{15}N-edited SQ—(*cyan*) or TQ—(*blue*) diffusion experiments; extracted diffusion constants of $(1.39\pm0.02)\times10^{-6}$, $(1.34\pm0.01)\times10^{-6}$ and $(1.37\pm0.02)\times10^{-6}$ cm^{2}s^{-1} are obtained, respectively. In **a** and **b** *dashed lines* are fits of the experimental data (*circles*) to a single exponential decay function (Eq. 3). The value Δ′ was set to be 0.15 s, with δ/2 = 1 ms and 0.33 ms for SQ- and TQ-experiments, respectively. **c** As in (**a, b**) but for U-^{2}H, Ileδ1[$^{13}CH_3$], Leu,Val-[$^{13}CH_3$,$^{12}CD_3$], Met-[$^{13}CH_3$]-$\alpha_7\alpha_7$ (360 kDa) with diffusion constants measured via SQ (*red*) and TQ (*blue*) experiments, 25 °C; extracted values of $(3.44\pm0.07)\times10^{-7}$ and $(3.63\pm0.07)\times10^{-7}$ cm^{2}s^{-1} are obtained, respectively, with all gradients along the *z*-axis. When the encoding/decoding gradients are along the *x*-axis (*inset*) the extracted diffusion constants are within 2% of each other for SQ and TQ approaches. Δ′ is set to 0.15 s, with δ/2 = 2 ms (SQ) and 0.667 ms (TQ). **d** Linear correlation plot of diffusion constants measured by SQ—(*x*-axis) and TQ—(*y*-axis) schemes for Ddx4$_{14FtoA}$ over a range of concentrations (10, 24, 38, 75, 145 and 250 mg/mL), 30 °C

integrating 1D spectra as a function of encoding/decoding gradient strengths, obtained for both TQ and SQ measurements. A high level of agreement is obtained between the two approaches, as can be seen by the near superposition of the intensity profiles. The diffusion constants measured via the different schemes are tabulated in the legend to Fig. 2. As expected, slight differences for diffusion constants for the different protein L samples were obtained, that reflects the approximately 20% higher viscosity of D_2O buffer ([Ile,Leu,Val-$^{13}CH_3$]-labeled sample) relative to 90%H_2O/10%D_2O, 25 °C, that was the solvent for the uniformly-labeled sample. As a second test we focused on a much larger protein system, corresponding to the 360 kDa half proteasome. Figure 2c shows profiles obtained from SQ and TQ experiments, which again highlight the good agreement between the two methods. Notably, the small discrepancy (~7%) in calculated diffusion constants from the two methods is reduced to within experimental error (<2%) when *x*-gradients are substituted for *z*-gradients for encoding/decoding, while the remaining gradients are left as *z* (inset to Fig. 2c) or when all *z* gradients are replaced by *x*. We have noted that, at least on our system,

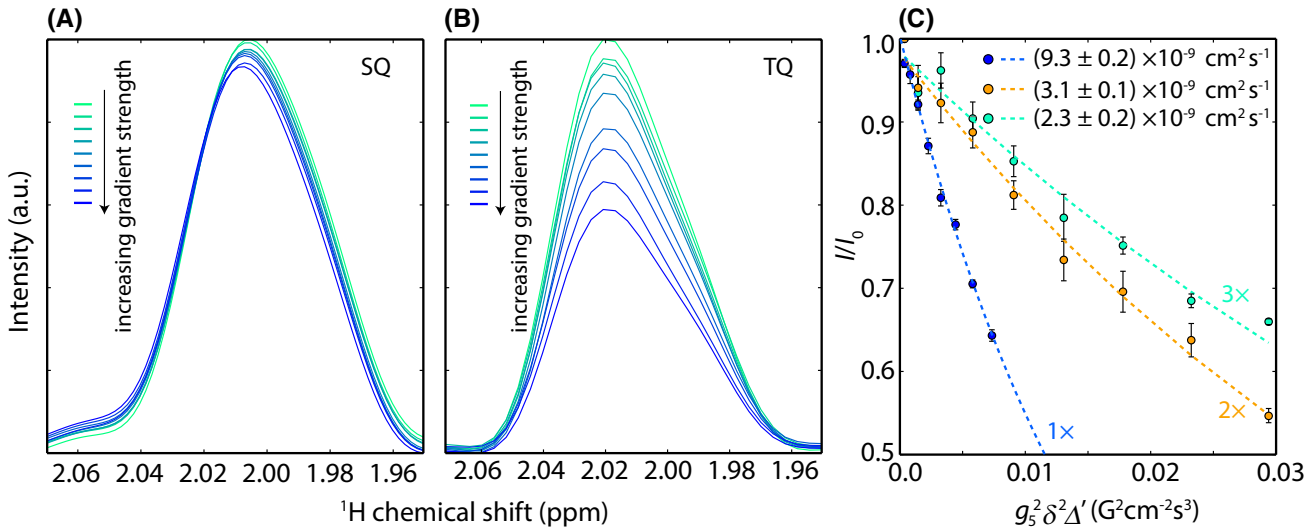

Fig. 3 Attenuation of superimposed methionine resonances from a condensed phase sample as a function of increased gradient strength in SQ—(**a**) and TQ—(**b**) experiments, 30 °C; Δ′ and δ/2 are set to 0.4 s and 2 ms, respectively, in the measurements. **c** Intensity profiles from diffusion measurements of Ddx4 (*blue*), Ddx4$_{2x}$ (*yellow*) and Ddx4$_{3x}$ (*teal*) as a function of $g_5^2\delta^2\Delta'$. The respective diffusion constants of the samples (35 °C) are labeled on the graph. (Δ′, δ/2) are set to (0.28 s, 2 ms) for Ddx4 and (0.5 s, 3 ms) for Ddx4$_{2x}$ and Ddx4$_{3x}$. The gradient strengths used are 4.5, 9.0, 13.5, 18.0, 22.5, 27.0, 31.5, 36.0, 40.5 Gauss cm^{-1}

using *x*- or *y*-gradients for encoding/decoding seems to be slightly more robust for measuring slow diffusion, although with the exception of applications to $\alpha_7\alpha_7$ all measurements were performed with *z*-gradients exclusively. The reason for this difference is unclear to us presently. As a final test we measured self-diffusion constants of a mutant of the N-terminal intrinsically disordered domain of Ddx4 in which all 14 Phe residues in the 236-residue construct were replaced by Ala, Ddx4$_{14FtoA}$. Unlike the wild-type version of the protein this variant does not phase separate under our experimental conditions (Nott et al. 2015). We have chosen protein concentrations from 10 to 250 mg/mL (10, 24, 38, 75, 145 and 250 mg/mL) that provide a range of diffusion rates that can be accurately quantified using both SQ and TQ experiments. Figure 2d shows a linear correlation plot of diffusion constants obtained in this manner, with excellent agreement between the two approaches.

Having established the utility of the methodology we next focused on an application where the SQ experiment fails, involving measurement of the self-diffusion of Ddx4 in a phase-separated condensed droplet (Nott et al. 2015). Figure 3a shows a small region from a series of SQ diffusion spectra recorded on wild-type Ddx4 using encoding/decoding gradients of 4 ms net duration and Δ′ = 400 ms, focusing on the Met region. It is noteworthy that Ddx4 is intrinsically disordered (Brady et al. 2017) so that all the Met methyl signals in the protein superimpose, providing a high sensitivity data set. Of interest, little decay in intensity (<5%) is observed as a function of gradient strength. By contrast, much more decay (40%) is noted in the case of the TQ experiment, Fig. 3b, enabling the reliable extraction of the diffusion constant ($7.8 \pm 0.4 \times 10^{-9}$ cm^{2}s^{-1}, 30 °C). The TQ pulse sequence has also been applied to the measurement of diffusion rates for slower diffusing systems as well. Here we have focused on N- to C-terminal concatenated Ddx4 units (residues 1-236), Ddx4$_{2x}$ and Ddx4$_{3x}$, where the subscript refers to the number of units. Both Ddx4$_{2x}$ and Ddx4$_{3x}$ form condensed phase liquid droplets (300–400 mg/mL) from which we were able to extract self-diffusion coefficients as low as ($2.3 \pm 0.2) \times 10^{-9}$ cm^{2}s^{-1} (Ddx4$_{3x}$, 35 °C). Finally, we have tested for the presence of convection by recording experiments with different diffusion delays, Δ′, ranging from 0.15 to 0.4 s. Diffusion constant values within 1–2% of each other were obtained.

In summary, we have presented a TQ-based pulse scheme for the accurate measurement of small diffusion coefficients, on the order of 10^{-9} cm^{2}s^{-1}. The utility of the approach has been demonstrated on a number of protein systems, including the phase separated state of Ddx4. It is anticipated that studies of self-diffusion of molecular constituents of phase separated droplets will provide important insights into the origin of the forces that stabilize these membraneless organelles and that the TQ experiment will prove useful in this regard.

Acknowledgements This work was supported by grants from the Canadian Institutes of Health Research and the Natural Sciences and Engineering Research Council of Canada. L.E.K holds a Canada Research Chair in Biochemistry.

References

Ahuja P, Sarkar R, Vasos PR, Bodenhausen G (2009) Diffusion coefficients of biomolecules using long-lived spin states diffusion coefficients of biomolecules using long-lived spin states. J Am Chem Soc 131:7498–7499. doi:10.1021/ja902030k

Bouvignies G, Kay LE (2012) A 2D ^{13}C-CEST experiment for studying slowly exchanging protein systems using methyl probes: an application to protein folding. J Biomol NMR 53:303–310. doi:10.1007/s10858-012-9640-7

Brady JP, Farber PJ, Sekhar A, et al (2017) Structural and hydrodynamic properties of an intrinsically disordered region of a germ-cell specific protein upon phase separation. (submitted).

Brangwynne CP, Tompa P, Pappu RV (2015) Polymer physics of intracellular phase transitions. Nat Phys 11:899–904. doi:10.1038/nphys3532

Buevich AV, Baum J (2002) Residue-specific real-time NMR diffusion experiments define the association states of proteins during folding. J Am Chem Soc 124:7156–7162. doi:10.1021/ja012699u

Choy WY, Mulder FA, Crowhurst KA et al (2002) Distribution of molecular size within an unfolded state ensemble using small-angle X-ray scattering and pulse field gradient NMR techniques. J Mol Biol 316:101–112. doi:10.1006/jmbi.2001.5328

Dehner A, Kessler H (2005) Diffusion NMR spectroscopy: folding and aggregation of domains in p53. ChemBioChem 6:1550–1565. doi:10.1002/cbic.200500093

Didenko T, Boelens R, Rüdiger SG (2011) 3D DOSY-TROSY to determine the translational diffusion coefficient of large protein complexes. Protein Eng Des Sel 24:99–103. doi:10.1093/protein/gzq091

Dingley AJ, Mackay JP, Chapman BE et al (1995) Measuring protein self-association using pulsed-field-gradient NMR spectroscopy: application to myosin light chain 2. J Biomol NMR 6:321–328. doi:10.1007/BF00197813

Hajduk PJ, Olejniczak ET, Fesik SW (1997) One-dimensional relaxation- and diffusion-edited NMR methods for screening compounds that bind to macromolecules. J Am Chem Soc 119:12257–12261. doi:10.1021/ja9715962

Horst R, Horwich AL, Wüthrich K (2011) Translational diffusion of macromolecular assemblies measured using transverse-relaxation-optimized pulsed field gradient NMR. J Am Chem Soc 133:16354–16357. doi:10.1021/ja206531c

Huang R, Ripstein ZA, Augustyniak R et al (2016) Unfolding the mechanism of the AAA+ unfoldase VAT by a combined cryo-EM, solution NMR study. Proc Natl Acad Sci USA 113:E4190–E4199. doi:10.1073/pnas.1603980113

Johnson Jr CS (1999) Diffusion ordered nuclear magnetic resonance spectroscopy: principles and applications. Prog Nucl Magn Reson Spectrosc 34:203–256. doi:10.1016/S0079-6565(99)00003-5

Kay LE, Prestegard JH (1986) An application of pulse-gradient double-quantum spin echoes to diffusion measurements on molecules with scalar-coupled spins. J Magn Reson 67:103–113. doi:10.1016/0022-2364(86)90413-0

Levitt MH, Freeman R (1979) NMR population inversion using a composite pulse. J Magn Reson 33:473–476. doi:10.1016/0022-2364(79)90265-8

Martin JF, Selwyn LS, Vold RR, Vold RL (1982) The determination of translational diffusion constants in liquid crystals from pulsed field gradient double quantum spin echo decays. J Chem Phys 76:2632–2634. doi:10.1063/1.443243

Mittermaier A, Kay LE (2001) X1 torsion angle dynamics in proteins from dipolar couplings. J Am Chem Soc 123:6892–6903. doi:10.1021/ja010595d

Nott TJ, Petsalaki E, Farber P et al (2015) Phase transition of a disordered nuage protein generates environmentally responsive membraneless organelles. Mol Cell 57:936–947. doi:10.1016/j.molcel.2015.01.013

Price WS (1998) Pulsed-field gradient nuclear magnetic resonance as a tool for studying translational diffusion: part II. Experimental aspects. Concepts Magn Reson 10:197–237. doi:10.1002/(SICI)1099-0534

Price WS, Tsuchiya F, Arata Y (1999) Lysozyme aggregation and solution properties studied using PGSE NMR diffusion measurements. J Am Chem Soc 121:11503–11512. doi:10.1021/ja992265n

Sekhar A, Rosenzweig R, Bouvignies G, Kay LE (2015) Mapping the conformation of a client protein through the Hsp70 functional cycle. Proc Natl Acad Sci USA 112:10395–10400. doi:10.1073/pnas.1508504112

Sklenar V, Piotto M, Leppik R, Saudek V (1993) Gradient-tailored water suppression for ^{1}H–^{15}N HSQC experiments optimized to retain full sensitivity. J Magn Reson Ser A 102:241–245. doi:10.1006/jmra.1993.1098

Sprangers R, Kay LE (2007) Quantitative dynamics and binding studies of the 20S proteasome by NMR. Nature 445:618–622. doi:10.1038/nature05512

Stejskal EO, Tanner JE (1965) Spin diffusion measurements: spin echoes in the presence of a time-dependant field gradient. J Chem Phys 42:288–292. doi:10.1063/1.1695690

Tanner JE (1970) Use of the stimulated echo in NMR diffusion studies. J Chem Phys 52:2523–2526. doi:10.1063/1.1673336

Weljie AM, Yamniuk AP, Yoshino H et al (2003) Protein conformational changes studied by diffusion NMR spectroscopy: application to helix-loop-helix calcium binding proteins. Protein Sci 12:228–236. doi:10.1110/ps.0226203

Yan J, Kline AD, Mo H et al (2002) Epitope mapping of ligand-receptor interactions by diffusion NMR. J Am Chem Soc 124:9984–9985. doi:10.1021/ja0264347

Yao S, Weber DK, Separovic F, Keizer DW (2014) Measuring translational diffusion coefficients of peptides and proteins by PFG-NMR using band-selective RF pulses. Eur Biophys J 43:331–339. doi:10.1007/s00249-014-0965-x

Zax D, Pines A (1983) Study of anisotropic diffusion of oriented molecules by multiple quantum spin echoes. J Chem Phys 78:6333–6334. doi:10.1063/1.444559

Zheng G, Torres AM, Price WS (2009) MQ-PGSTE: a new multi-quantum STE-based PGSE NMR sequence. J Magn Reson 198:271–274. doi:10.1016/j.jmr.2009.03.004